Analysis of the degrees-of-freedom of spatial parallel manipulators in regular and singular configurations

R Arun Srivatsan[1], Sandipan Bandyopadhyay[2], Ashitava Ghosal[3]

Abstract

This paper presents a study of the nature of the degrees-of-freedom of spatial manipulators based on the concept of partition of degrees-of-freedom. In particular, the partitioning of degrees-of-freedom is studied in five lower-mobility spatial parallel manipulators possessing different combinations of degrees-of-freedom. An extension of the existing theory is introduced so as to analyse the nature of the gained degree(s)-of-freedom at a gain-type singularity. The gain of one- and two-degrees-of-freedom is analysed in several well-studied, as well as newly developed manipulators. The formulations also present a basis for the analysis of the velocity kinematics of manipulators of any architecture.

Keywords: Parallel manipulators, instantaneous degrees-of-freedom, singularity, lower-mobility manipulators.

1. Introduction

Spatial manipulators were originally designed to have all of the possible six-degrees-of-freedom (DoF). The famous PUMA [1] or the Stewart platform manipulators [2] represent this trend. While these manipulators have proven to be versatile in terms of handling a large range of tasks by virtue of their *full-mobility*, they turned out to be relatively expensive for the same reason. Moreover, in a large number of applications where only a subset of the six-DoF sufficed, the manipulators' capabilities would appear to be

[1]Department of Engineering Design, Indian Institute of Technology Madras, email: rarunsrivatsan@gmail.com

[2]Corresponding author, Department of Engineering Design, Indian Institute of Technology Madras, Chennai 600 036, India; Phone: +91 44 2257 4733, email: sandipan@iitm.ac.in

[3]Department of Mechanical Engineering, Indian Institute of Science, Bangalore, India, email:asitava@mecheng.iisc.ernet.in

practically redundant. It is for these reasons, that a large number of manipulators with "lower-mobility", i.e., less than six-DoF, have come up in the past few decades: the SCARA [3], the DELTA [4], the 3-R$\underline{P}$S [5], the cylindrical manipulator [6], the 3-U$\underline{P}$U [7], the Agile Eye [8], the CaPaMan [9] and the MaPaMan [10], to name a few. Most of these manipulators are designed for a particular set of tasks. For example, the Agile Eye, as the name suggests, provides a dexterous camera mount with spherical motion capability; the DELTA, on the other hand, provides three translational motions, making it very successful in operations such as "pick-and-place" in the industries. The motion analysis of these two manipulators, and others with similar motions, is relatively easy, for their workspaces form not only proper subsets of $SE(3)$ (i.e., the special Euclidean group signifying the space of general displacements of the rigid bodies), these are actually *sub-groups* of the same – $SO(3)$ in the case of Agile Eye,(i.e., the special orthogonal group signifying the space of rigid body rotations) and $\mathbb{R}^3$ for DELTA (i.e., space of pure translations). Understanding the motion of other manipulators, such as the 3-R$\underline{P}$S and MaPaMan, is more challenging, for these three-DoF manipulators do not belong to either *spherical*, or *Cartesian* categories. Instead, their platforms can show motions which are combinations of rotation(s), as well as translation(s). For instance, the 3-R$\underline{P}$S manipulator, even though originally designated as a *parallel wrist*, actually possesses *two* rotational, and *one* translational DoF [11].

The study of the DoF or mobility of linkages and manipulators has a long history. In [12], Gogu has presented a summary of the important developments up to the year 2005. His analysis of a significant number of existing mobility criteria showed that simple calculations based on the topology of the mechanisms alone were not always reliable in predicting even the actual DoF itself. Thus, the problem of determination of the nature and distribution of the DoF in a comprehensive manner is not addressed by these classical methods. Towards this goal, researchers have employed methods based on *instantaneous kinematics*. A popular approach in this category is the application of screw theory. For a three-DoF parallel manipulator, the *three-system* of screws to which the resultant twist of the moving platform belongs, can be formulated. Then, the *principal screws* of this system can be computed, leading to the identification of the distinct screw-system to which the motion belongs, as per the classification given in [13, 14]. This is the approach used in [15] for the analysis of the 3-R$\underline{P}$S manipulator.

An inherent drawback of such analyses is that the results are not *global*, i.e., all the conclusions relate only to the configuration under consideration, which can change with the motion of the manipulator. In addition, some practical as well as conceptual difficulties present themselves in this type

of analyses. Firstly, unlike in the case of serial manipulators, the *twists* of the end-effectors of parallel manipulators are difficult to find. In fact, there is no standard or uniform formulation followed by the researchers, leading to a significant degree of diversity at this preparatory step itself. In order to circumvent this problem, one approach takes advantage of the fact that the computation of the input *wrenches* is generally easier than the input twists, and that these systems are *reciprocal*, to analyse the wrench system for determining the nature of the twists [16, 17]. Even with all these steps, when the end-result is obtained, i.e., the screw-system is identified, it does not specify, in an explicit manner, how the total DoF of the platform is *partitioned* in rotational and translational DoF.

In the recent years, another approach has come up to address some of these issues. In this approach, a slightly different point of view is adopted, and the space of the twists is analysed *directly*, as opposed to the underlying space of screws. One formulation involves composing a Jacobian matrix and finding the dimension of its nullspace [18]. Another leads to the eigenproblem of a *symmetric positive-semidefinite* matrix of dimension $n \times n$, n being the DoF of the motion under consideration [11, 19]. The rank of this matrix indicates the number of rotational DoF. Since this number can be three at the most, the eigenproblem leads to a characteristic polynomial whose non-trivial factor is *at the most* a cubic. The coefficients of this cubic, and therefore its roots can be computed analytically in *closed-form*, in principle[4]. Thus, the rotational DoF can be identified accurately. Using the eigenvectors corresponding to the vanishing eigenvalues, one can obtain the number of translational DoF as well. Following this analysis, a new classification of generic motion of a rigid-body has been presented, based solely on the DoF characteristic [19, 20]. In this paper, this method of analysis and classification is followed to understand the motion characteristics of a number of three-DoF spatial parallel manipulators. Such manipulators can have either 3, 2, 1 or 0 linearly independent rotational DoF, and 0, 1, 2 or 3 translational DoF, respectively – leading to four distinct classes within this type of manipulators.

It is well-known that the DoF of a parallel manipulator is subject to change at a singularity. The manipulator *gains* one or more DoF at a *gain-type* singularity, and similarly, loses one or more DoF at a *loss-type* singularity. While the *lost* DoF is easy to identify (from the generic analysis of the DoF at such a singularity), the analysis of the *gained motion* requires a more involved treatment. Various methods to identify and interpret the

[4]In most practical problems, however, the symbolic expressions involved are too large to be amenable to analysis, and thus one is forced to introduce numbers into them.

gained motion already exist in literature (see, e.g., [21, 22] and the references therein). However, a systematic study of the same, for the class of manipulators described here, is not available to the best of the knowledge of the authors. This paper attempts to present such an analysis. It describes a generic method to derive the required mathematical elements (i.e., the Jacobian matrices) for a generic platform-type manipulator, and uses these for the analysis of the DoF of a number of three-DoF spatial parallel manipulators, at generic as well as singular configurations. It establishes, perhaps for the first time, a method of analysis of the nature of the gained DoF, when a manipulator gains *more than one* DoF at a singularity.

The rest of the paper is organised as follows: in Section 2, the formulation for the analysis of DoF in the non-singular configurations is presented, followed by a similar analysis of the gained-DoF in the singular configurations in Section 3. In Sections 4 and 5, the formulations are applied to several three-DoF spatial parallel manipulators, in the non-singular and singular configurations, respectively. Finally, the conclusions are presented in Section 6.

2. Formulation for the non-singular cases

The methodology for computing the partitioning of the DoF of a rigid-body in motion has been described in [11, 19, 20]. Some relevant parts of it, in particular, elements specific to parallel manipulators, are described in the following.

2.1. Definition of the different Jacobian matrices

As the method analyses *instantaneous* properties of the motion of a rigid body, a number of Jacobian matrices come into play. Furthermore, the body in question is the *end-effector* of a parallel manipulator, and as such its motion is *constrained* by the *loop-closure* conditions in a parallel manipulator. These constraints are also incorporated in the motion of the end-effector[5] by means of the corresponding Jacobian matrices. The derivation of these matrices are described in the following.

2.1.1. Equivalent linear velocity Jacobian, $\boldsymbol{J}_{\boldsymbol{v}}^{eq}$

The linear velocity Jacobian is computed based on the position of a *point of interest* on the moving platform. In general, the position vector of this

[5]In parallel manipulators, the choice of the output link (or the end-effector) is not so obvious always. In this paper, only *platform-type* manipulators are studied, leading to the obvious choice of the platform as the end-effector in all the cases.

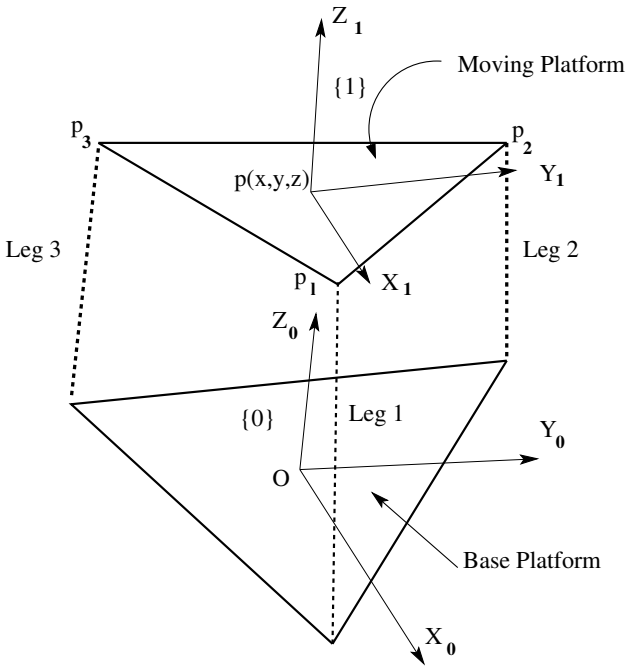

Figure 1: Schematic representation of three-DoF parallel manipulator with three legs

point may be obtained as a linear combination of the vertices of the moving platform:

$$^0\boldsymbol{p} = \sum_{i=1}^{s} a_i^0 \boldsymbol{p}_i, \;\; a_i \in \mathbb{R}, \tag{1}$$

where $^0\boldsymbol{p}_i$ $(i = 1, \ldots, s)$, denote the position vectors of the vertices of the mobile platform in the *global* frame of reference and s is the number of vertices (see Fig. 1). The velocity of the point $^0\boldsymbol{p}$ is written in terms of the corresponding Jacobian as:

$$^0\boldsymbol{v}_{\boldsymbol{p}} = \frac{d^0\boldsymbol{p}}{dt} = \frac{\partial^0\boldsymbol{p}}{\partial \boldsymbol{q}}\dot{\boldsymbol{q}}, \tag{2}$$

where $\boldsymbol{q}$ represents the vector of *configuration variables*, defining the configuration of the manipulator *uniquely*. For a parallel manipulator, it is always possible to partition $\boldsymbol{q}$ as $\boldsymbol{q} = (\boldsymbol{\theta}^T, \boldsymbol{\phi}^T)^T$, where $\boldsymbol{\theta} \in \mathbb{R}^n$ represents the vector of the actuated or *active* joint variables, and $\boldsymbol{\phi} \in \mathbb{R}^m$ the non-actuated or *passive* ones (see, e.g., [21]). Thus, Eq. (2) may be rewritten as:

$$^0\boldsymbol{v}_{\boldsymbol{p}} = \frac{d^0\boldsymbol{p}}{dt} = \boldsymbol{J}_{\boldsymbol{p\theta}}\dot{\boldsymbol{\theta}} + \boldsymbol{J}_{\boldsymbol{p\phi}}\dot{\boldsymbol{\phi}}, \quad \text{where } \boldsymbol{J}_{\boldsymbol{p\theta}} = \frac{\partial^0\boldsymbol{p}}{\partial\boldsymbol{\theta}}, \text{ and } \boldsymbol{J}_{\boldsymbol{p\phi}} = \frac{\partial^0\boldsymbol{p}}{\partial\boldsymbol{\phi}}. \tag{3}$$

In order to *transfer* the effects of the motions of the passive links to those of the active ones, the passive joint rate, $\dot{\boldsymbol{\phi}}$, needs to be computed. This is done by differentiating the loop-closure equations, $\boldsymbol{\eta}(\boldsymbol{\theta}, \boldsymbol{\phi}) = \mathbf{0}$ [22] to obtain the following:

$$\boldsymbol{J}_{\boldsymbol{\eta\theta}}\dot{\boldsymbol{\theta}} + \boldsymbol{J}_{\boldsymbol{\eta\phi}}\dot{\boldsymbol{\phi}} = \mathbf{0}, \quad \text{where} \tag{4}$$

$$\boldsymbol{J}_{\boldsymbol{\eta\theta}} = \frac{\partial \boldsymbol{\eta}}{\partial \boldsymbol{\theta}}, \ \boldsymbol{J}_{\boldsymbol{\eta\phi}} = \frac{\partial \boldsymbol{\eta}}{\partial \boldsymbol{\phi}}. \tag{5}$$

$$\Rightarrow \dot{\boldsymbol{\phi}} = \boldsymbol{J}_{\boldsymbol{\phi\theta}}\dot{\boldsymbol{\theta}}, \quad \text{where} \tag{6}$$

$$\boldsymbol{J}_{\boldsymbol{\phi\theta}} = -\boldsymbol{J}_{\boldsymbol{\eta\phi}}\boldsymbol{J}_{\boldsymbol{\eta\theta}}, \quad \text{and } \det\left(\boldsymbol{J}_{\boldsymbol{\eta\phi}}\right) \neq 0. \tag{7}$$

Using Eq. (6) in Eq. (3), one obtains, finally,

$${}^{0}\boldsymbol{v}_{\boldsymbol{p}} = \boldsymbol{J}_{\boldsymbol{v}}^{eq}\dot{\boldsymbol{\theta}}, \quad \text{where} \tag{8}$$

$$\boldsymbol{J}_{\boldsymbol{v}}^{eq} = \boldsymbol{J}_{\boldsymbol{p\theta}} + \boldsymbol{J}_{\boldsymbol{p\phi}}\boldsymbol{J}_{\boldsymbol{\phi\theta}}. \tag{9}$$

This completes the derivation of the *equivalent linear velocity Jacobian* for *any* parallel or hybrid manipulator.

2.1.2. Equivalent angular velocity Jacobian, $\boldsymbol{J}_{\boldsymbol{\omega}}^{eq}$

Several approaches exist for the computation of the angular velocity of the moving platform of a platform-type manipulator. The one presented here is applicable to any platform-type parallel or hybrid manipulator, such as the one shown in Fig. 1. The approach depends on first obtaining the rotation matrix, ${}^{0}_{1}\boldsymbol{R}$, of the platform frame $\{1\}$ with respect to the fixed frame $\{0\}$.

The *space-fixed* angular velocity, in its matrix form, is given by the formula (see, e.g., [23], pp. 139):

$${}^{0}\boldsymbol{\Omega}_{s} = {}^{0}_{1}\dot{\boldsymbol{R}}({}^{0}_{1}\boldsymbol{R})^{T} \in so(3), \tag{10}$$

where $so(3)$ is the space of angular velocity matrices [24]. Extracting the vector ${}^{0}\boldsymbol{\omega}_{s}$ from the skew-symmetric matrix ${}^{0}\boldsymbol{\Omega}_{s}$, one gets:

$${}^{0}\boldsymbol{\omega}_{s} = ({}^{0}\boldsymbol{\Omega}_{s})^{\vee} \in \mathbb{R}^{3}, \tag{11}$$

where $(\cdot)^{\vee} : so(3) \rightarrow \mathbb{R}^{3}$ is an operator such that $\boldsymbol{\Omega a} = \boldsymbol{\omega} \times \boldsymbol{a} \ \forall \boldsymbol{a} \in \mathbb{R}^{3}$, where $\boldsymbol{\omega} = \boldsymbol{\Omega}^{\vee}$ (see, e.g., [24]). Separating the coefficients of $\dot{\boldsymbol{\theta}}$ and $\dot{\boldsymbol{\phi}}$, one gets an expression for the angular velocity similar to that of the linear velocity in Eq. (3):

$${}^{0}\boldsymbol{\omega}_{s} = \boldsymbol{J}_{\boldsymbol{\omega\theta}}\dot{\boldsymbol{\theta}} + \boldsymbol{J}_{\boldsymbol{\omega\phi}}\dot{\boldsymbol{\phi}}. \tag{12}$$

Once again, replacing $\dot{\boldsymbol{\phi}}$ by $\boldsymbol{J}_{\boldsymbol{\phi\theta}}\dot{\boldsymbol{\theta}}$, the final expression for the *equivalent Jacobian matrix for the angular velocity* is obtained as:

$$^0\boldsymbol{\omega}_s = \boldsymbol{J}^{eq}_{\boldsymbol{\omega}}\dot{\boldsymbol{\theta}}, \quad \text{where } \boldsymbol{J}^{eq}_{\boldsymbol{\omega}} = \boldsymbol{J}_{\boldsymbol{\omega\theta}} + \boldsymbol{J}_{\boldsymbol{\omega\phi}}\boldsymbol{J}_{\boldsymbol{\phi\theta}}. \tag{13}$$

2.2. Analysis of the nature of DoF

Once the Jacobian matrices are formed, the analysis of the DoF can be done by means of the solution of an eigenvalue problem, as shown in [11]. Though the results therein have been derived through the use of dual-number algebra, it is possible to perform the computations within the framework of real algebra alone. The computational steps are summarised below:

1. Form the matrix $\boldsymbol{g} = (\boldsymbol{J}^{eq}_{\boldsymbol{\omega}})^T\boldsymbol{J}^{eq}_{\boldsymbol{\omega}} \in \mathbb{R}^{n\times n}$.
2. Solve the eigenproblem of $\boldsymbol{g}$, so as to obtain the eigenvalues λ_i, and the corresponding eigenvectors $\dot{\boldsymbol{\theta}}_i \forall\ i = 1, \ldots, n$.
3. Count the *independent* rotational DoF from the number of *non-zero* eigenvalues. This number can be *at the most* 3 for any positive integer n, since $\text{rank}(\boldsymbol{J}^{eq}_{\boldsymbol{\omega}}) \leq 3$.
4. Find the eigenvectors (denoted by $\dot{\boldsymbol{\theta}}^N_i$) corresponding to the zero-valued eigenvalues, from the solution of the following equation:

$$\boldsymbol{g}\dot{\boldsymbol{\theta}}^N_i = \boldsymbol{0},\ i = 1, \ldots, n_g, \quad \text{where } n_g = \text{nullity}(\boldsymbol{g}). \tag{14}$$

5. Form the matrix $\boldsymbol{J}_{\boldsymbol{V}}$, such that the ith column of it is given by the vector $\boldsymbol{J}^{eq}_{\boldsymbol{v}}\dot{\boldsymbol{\theta}}^N_i$, i.e.,

$$\boldsymbol{J}_{\boldsymbol{V}} = \left[\, \boldsymbol{J}^{eq}_{\boldsymbol{v}}\dot{\boldsymbol{\theta}}^N_1 \,\middle|\, \boldsymbol{J}^{eq}_{\boldsymbol{v}}\dot{\boldsymbol{\theta}}^N_2 \,\middle|\, \cdots \,\middle|\, \boldsymbol{J}^{eq}_{\boldsymbol{v}}\dot{\boldsymbol{\theta}}^N_{n_g} \,\right].$$

   The rank of $\boldsymbol{J}_{\boldsymbol{V}}$ represents the number of independent translational motions, while the difference between $\text{rank}(\boldsymbol{J}^{eq}_{\boldsymbol{v}})$ and $\text{rank}(\boldsymbol{J}_{\boldsymbol{V}})$ represents the number of dependent (or parasitic) translational motions.
6. Form the matrix $\boldsymbol{g}_{\boldsymbol{V}} = \boldsymbol{J}^T_{\boldsymbol{V}}\boldsymbol{J}_{\boldsymbol{V}}$.
7. Find the $\text{rank}(\boldsymbol{g}_{\boldsymbol{V}})$ by solving its eigenproblem or otherwise.
8. Finally, the total *instantaneous* DoF is obtained from the formula:

$$\text{DoF} = \text{rank}(\boldsymbol{g}) + \text{rank}(\boldsymbol{g}_{\boldsymbol{V}}). \tag{15}$$

   In the above formula, the first term in the RHS indicates the *rotational DoF* and the second term gives the *purely translational DoF*. This process is followed in the analysis of the DoF of a number of 3-DoF spatial parallel manipulators in Section 4.

3. Analysis of the gained-DoF at singularities

It is well-known in literature that *all* manipulators lose one or more DoF at a *loss-type* singularity, while a parallel or hybrid manipulator can also *gain* DoF at a *gain-type* singularity [21]. The *number* of gained or lost DoF can be easily computed based on the rank of certain Jacobian matrices [21, 22]. Identification of the *nature* of the lost or gained DoF needs further analysis. In the case of a loss of DoF, the steps mentioned in Section 2.2 need to be followed to analyse the *remaining* DoF. The procedure for the gained DoF is more involved. It is explained in the following.

It is clear that the above formulation of the Jacobian matrices hold under the condition:

$$\det(\boldsymbol{J}_{\boldsymbol{\eta\phi}}) \neq 0. \tag{16}$$

When this is violated, the manipulator is said to be at a *constraint-* or *gain-*type singularity. It is customary to investigate the motion arising out of the *gained* DoF alone (see, e.g., [11, 21]). In order to do so, the gained passive velocity is found out first, while the actuators are held fixed, i.e., $\dot{\boldsymbol{\theta}} = \mathbf{0}$. In such a case, Eq. (3) reduces to:

$$\boldsymbol{J}_{\boldsymbol{\eta\phi}}\dot{\boldsymbol{\phi}}_i^N = \mathbf{0},\ i = 1, \ldots, n_{\mathrm{s}}, \quad \text{where } n_{\mathrm{s}} = \text{nullity}(\boldsymbol{J}_{\boldsymbol{\eta\phi}}). \tag{17}$$

The gained angular and linear velocities can be obtained as:

$${}^0\boldsymbol{\omega}_i^N = \boldsymbol{J}_{\boldsymbol{\omega\phi}}\dot{\boldsymbol{\phi}}_i^N \tag{18}$$

$${}^0\boldsymbol{v}_i^N = \boldsymbol{J}_{\boldsymbol{v\phi}}\dot{\boldsymbol{\phi}}_i^N,\ i = 1, \ldots, n_{\mathrm{s}}. \tag{19}$$

Eqs. (18,19) imply that even with the actuators locked the end-effector of the parallel manipulator can *instantaneously* have non-zero linear and/or angular velocity(ies) – owing to the gained DoF.

If there is the gain of only one DoF, i.e., $n_s = 1$, then there are only two possibilities: the gained motion can be rotational in nature, i.e., the motion belongs to the class $\boldsymbol{\chi}_{10}$, when $\|\boldsymbol{\omega}_1^N\| \neq 0$; otherwise, the motion is purely translational in nature, i.e., it belongs to the class $\boldsymbol{\chi}_{01}$ [20] (see Appendix A).

When $n_s \geq 2$, the analysis can be carried out in a manner analogous to the study of $\boldsymbol{g}$. The steps involved are described below:

1. Construct the matrix $\boldsymbol{J}_{\boldsymbol{\omega}}^N$ such that the ith column of it is given by the vector $\boldsymbol{\omega}_i^N$ as defined in Eq. (18):

$$\boldsymbol{J}_{\boldsymbol{\omega}}^N = \left[\, \boldsymbol{J}_{\boldsymbol{\omega\phi}}\dot{\boldsymbol{\phi}}_1^N \,\middle|\, \boldsymbol{J}_{\boldsymbol{\omega\phi}}\dot{\boldsymbol{\phi}}_2^N \,\middle|\, \cdots \,\middle|\, \boldsymbol{J}_{\boldsymbol{\omega\phi}}\dot{\boldsymbol{\phi}}_{n_s}^N \,\right].$$

   This matrix is analogous to $\boldsymbol{J}_{\boldsymbol{\omega}}^{eq}$, except that it relates to the angular velocities arising out of the gained DoF *alone*.

2. Compute $\boldsymbol{g}^N = (\boldsymbol{J}^N_{\boldsymbol{\omega}})^T \boldsymbol{J}^N_{\boldsymbol{\omega}}$. This matrix is analogous to $\boldsymbol{g}$ in the same way as $\boldsymbol{J}^N_{\boldsymbol{\omega}}$ relates to $\boldsymbol{J}^{eq}_{\boldsymbol{\omega}}$.
3. Solve the eigenproblem of $\boldsymbol{g}^N$. The number of non-zero eigenvalues indicate the number of *gained rotational DoF*.
4. Construct the matrix $\boldsymbol{J}^N_{\boldsymbol{V}}$ such that the ith column of it is given by the vector $\boldsymbol{v}^N_i$ as defined in Eq. (19). This matrix is analogous to $\boldsymbol{J}^{eq}_{\boldsymbol{v}}$ in the non-singular case.
5. Map the nullspace of $\boldsymbol{g}^N$ by the matrix $\boldsymbol{J}^N_{\boldsymbol{v}}$ to get the matrix $\boldsymbol{J}^N_{\boldsymbol{V}}$.
6. Compute the matrix $\boldsymbol{g}^N_V = (\boldsymbol{J}^N_{\boldsymbol{V}})^T \boldsymbol{J}^N_{\boldsymbol{V}}$.
7. Find the rank$(\boldsymbol{g}^N_V)$ by solving its eigenproblem or otherwise. This number defines the number of *gained translational DoF*.
8. Finally, find the actual gained DoF as:

$$\text{Gained DoF} = \text{rank}(\boldsymbol{g}^N) + \text{rank}(\boldsymbol{g}^N_V). \tag{20}$$

Note that the last step may appear as redundant, as one could expect the gained DoF to equal n_s in *all* the cases. However, this is not necessarily true. It may so happen that at a singular configuration the columns of $\boldsymbol{J}^N_{\boldsymbol{\omega}}$ are *linearly dependent* and/or so are those of $\boldsymbol{J}^N_{\boldsymbol{V}}$, in such a manner that the sum in Eq. (20) falls below its maximum possible value, given by n_s.

4. DoF partitioning for three-DoF parallel manipulators

The theory developed in Sections 2, 3 is illustrated with the help of five examples of three-DoF spatial parallel manipulators in this section. The manipulators chosen are: a) 3-R<u>P</u>S parallel manipulator [5], b) Agile Eye parallel manipulator [8], c) "cylindrical" manipulator [6], d) MaPaMan-I [10], and e) MaPaMan-II [10]. The first three manipulators are well known in literature, but detailed analysis regarding the partitioning of their DoF, and more specifically, the partitioning in singular cases are not entirely known. The last two have been introduced recently, and their partitioning in non-singular and singular configurations are only partially known.

4.1. The 3-R<u>P</u>S *manipulator*

The 3-R<u>P</u>S parallel manipulator was introduced in 1988 by Lee and Shah [5] and has since been studied extensively by several researchers. The manipulator, as shown in Fig. 2, consists of a fixed and a moving platform. The platforms are connected by means of three legs, each of which has a rotary, a prismatic, and a spherical joint. The prismatic joints are actuated, and all the other joints are passive. This gives rise to three-DoF for the moving platform. For the sake of convenience, the fixed base and moving top

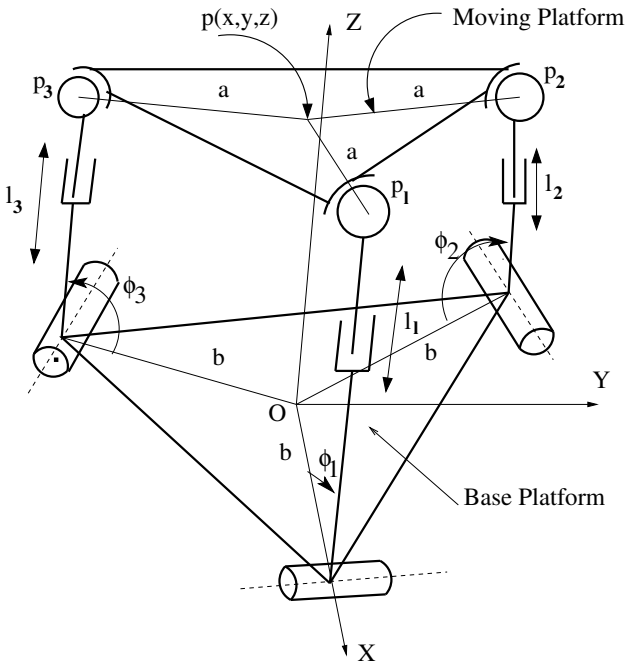

Figure 2: The 3-RPS manipulator

platforms are chosen as equilateral triangles circumscribed by circles of radii b and a respectively. The coordinates of the end-effector are obtained as:

$$
\begin{aligned}
{}^0\boldsymbol{p}_1 &= (b - l_1 \cos\phi_1, 0, l_1 \sin\phi_1)^T, \\
{}^0\boldsymbol{p}_2 &= \boldsymbol{R}_Z\,(2\pi/3)\,(b - l_1 \cos\phi_2, 0, l_1 \sin\phi_2)^T, \\
{}^0\boldsymbol{p}_3 &= \boldsymbol{R}_Z\,(4\pi/3)\,(b - l_1 \cos\phi_3, 0, l_1 \sin\phi_3)^T,
\end{aligned}
$$

where $\boldsymbol{R}_A(\alpha)$ denotes the rotation matrix for CCW rotation about axis $\boldsymbol{A}$ through an angle α. As the moving platform is equilateral in shape, the obvious choice of the point of interest ${}^0\boldsymbol{p}$ is the centroid of the triangle:

$$
{}^0\boldsymbol{p} = \frac{1}{3}\left({}^0\boldsymbol{p}_1 + {}^0\boldsymbol{p}_2 + {}^0\boldsymbol{p}_3\right).
$$

Given the input variables $\boldsymbol{\theta}$=$(l_1, l_2, l_3)^T$, there are three passive variables $\boldsymbol{\phi} = (\phi_1, \phi_2, \phi_3)^T$, which need to be solved for. The three constraint equations are given by $\boldsymbol{\eta} = \boldsymbol{0}$, where $\boldsymbol{\eta} = (\eta_1, \eta_2, \eta_3)^T$, and:

$$
\begin{aligned}
\eta_1 &= ({}^0\boldsymbol{p}_2 - {}^0\boldsymbol{p}_1) \cdot ({}^0\boldsymbol{p}_2 - {}^0\boldsymbol{p}_1) - 3a^2, \\
\eta_2 &= ({}^0\boldsymbol{p}_3 - {}^0\boldsymbol{p}_2) \cdot ({}^0\boldsymbol{p}_3 - {}^0\boldsymbol{p}_2) - 3a^2, \\
\eta_3 &= ({}^0\boldsymbol{p}_1 - {}^0\boldsymbol{p}_3) \cdot ({}^0\boldsymbol{p}_1 - {}^0\boldsymbol{p}_3) - 3a^2.
\end{aligned} \tag{21}
$$

Following [23], the solution of the forward kinematics problem is reduced to that of solving an 8-degree univariate polynomial equation. The length dimensions are all scaled with respect to b. For the parameter value[6] $a = 1/2$, two typical non-singular configurations are studied, leading to the following results:

- For active variables $\boldsymbol{\theta}=(1/2, 1, 2)^T$, the passive variables are given by $\boldsymbol{\phi}=(0.4, 0.753, 0.240)^T$. The matrix $\boldsymbol{J_\omega}$ is computed to be:

$$\boldsymbol{J_\omega} = \begin{bmatrix} 0.271 & 0.427 & -1.671 \\ 1.322 & 0.564 & -3.787 \\ -1.013 & 0.473 & 0.298 \end{bmatrix}.$$

  Subsequently, $\boldsymbol{g}$ is found as:

$$\boldsymbol{g} = \begin{bmatrix} 2.849 & 0.382 & -5.764 \\ 0.382 & 0.724 & -2.707 \\ -5.764 & -2.707 & 17.222 \end{bmatrix}.$$

  The eigenvalues of $\boldsymbol{g}$ are[7] calculated as: 0, 1.167 and 19.627, respectively. Thus, the number of *independent* rotational DoF in this configuration is found to be $\text{rank}(\boldsymbol{g}) = 2$.

  In order to compute the *independent* translational DoF, one may be tempted to compute the number of independent vectors in the linear velocity Jacobian, $\boldsymbol{J_v^{eq}}$. In this configuration,

$$\boldsymbol{J_v^{eq}} = \begin{bmatrix} -0.508 & 0.119 & 0.490 \\ 0.181 & -0.227 & 0.355 \\ 0.145 & 0.619 & 2.183 \end{bmatrix}.$$

  Eigenvalues of this matrix are: $-0.539, -0.317$, and 2.305 respectively. Thus, one may be lead to believe, that the manipulator has *three* independent translational velocities in this configuration. Such a conclusion would obviously be incorrect, as it would mean that the manipulator has a total of $2 + 3 = 5$ DoF at this configuration, whereas the DoF is known to be 3 in this case. In order to resolve this issue, the method

[6] All angles are in radians and all lengths are dimensionless unless mentioned otherwise explicitly.

[7] Any number with an absolute value less than 10^{-15} is approximated by zero throughout the paper, unless mentioned otherwise explicitly.

proposed in this paper is applied to the problem. Following step 4 in Section 2.2, the 1-dimensional nullspace of $\boldsymbol{g}$ is computed as:

$$\dot{\boldsymbol{\theta}}_1^N = (0.473, 0.832, 0.289)^T.$$

Using this vector in step 5, the matrix $\boldsymbol{J_V}$ is computed as:

$$\boldsymbol{J_V} = (0, 0, 1.215)^T.$$

Since there is a single non-zero vector in $\boldsymbol{J_V}$, there is no need for the computation of the matrix $\boldsymbol{g_V}$ and solving its eigenproblem in this case, as it is obvious that the number of independent translational DoF is $\text{rank}(\boldsymbol{g_V}) = \text{rank}(\boldsymbol{J_V}) = 1$. Thus, the application of Eq. (15) to this problem presents the correct resolution in this example, that *the sum of the independent translational DoF and the independent rotational DoF equals the total DoF of the manipulator at the configuration considered.*

- For $\boldsymbol{\theta}$=$(2, 5/2, 3/2)^T$ and the corresponding passive variables $\boldsymbol{\phi}$=$(1.283, 0.691, 1.075)^T$, the eigenvalues of $\boldsymbol{g}$ are: 0, 2.9, 8.409. The vector $\boldsymbol{J_V} = (0, 0, 0.690)^T$. The matrix

$$\boldsymbol{J_v^{eq}} = \begin{bmatrix} -1.864 & -0.412 & 0.549 \\ 0.182 & -0.719 & 0.323 \\ 0.314 & 0.639 & 0.330 \end{bmatrix},$$

whose eigenvalues are: $-0.723, -0.565, 0.669$, i.e., once again, $\boldsymbol{J_v^{eq}}$ is of full rank. However, the vector $\dot{\boldsymbol{\theta}}_1^N = (0.662, 0.439, 0.607)^T$, and $\boldsymbol{J_V} = (0, 0, 0.690)^T$. Therefore, there is no qualitative difference in the nature of the DoF in between the two configurations.

It is seen that in both the configurations the moving platform has instantaneously two rotational DoF and one pure translational DoF along the $\boldsymbol{Z}$ axis, i.e., it belongs to the class $\boldsymbol{\chi}_{21}$ in these configurations. These conclusions are consistent with similar results reported in [11, 20]. As explained in [20], the platform cannot have an angular velocity about the $\boldsymbol{Z}$ axis since $\boldsymbol{p}_i$ are confined to distinct vertical planes. The third DoF of the 3-RPS is thus constrained to be purely translational in nature, and such a translation can only take place along the $\boldsymbol{Z}$ axis.

This example demonstrates clearly a common issue with the kinematics of lower mobility manipulators, which is sometimes referred to as "parasitic motion" [25, 26]. The term is motivated by the fact that these motions do not contribute *directly* to the actual DoF of the manipulator; rather, they are

associated with these *principal* motions in a dependent manner. For instance, these could be linear motions arising out of the fact that the input twists associated with the rotational motions do not intersect at a point [26]. These motions can hamper the understanding of the DoF from the standpoint of velocity analysis. Depending upon the architecture of the manipulator, its configuration, and the choice of the point of reference for the analysis of the linear velocities (i.e., the choice of the point ${}^0\boldsymbol{p}$ in the present paper), one may get varying ranks for the linear velocity Jacobian, $\boldsymbol{J}_{\boldsymbol{v}}^{eq}$. In the present example, this rank was three, while the independent or *pure* translational DoF was just one. This discrepancy stems out of the fact that $\boldsymbol{J}_{\boldsymbol{v}}^{eq}$ is computed based on *a single chosen point*, and unlike $\boldsymbol{J}_{\boldsymbol{\omega}}$, it does not represent a generic property of the motion of the entire end-effector. On the other hand, the properties of $\boldsymbol{J}_{\boldsymbol{V}}$ are *generic* to the entire end-effector, and they clearly agree with the known results as well as physical intuition. While only one of the translational velocities of ${}^0\boldsymbol{p}$ can be designated as a "principal DoF" or an element of the "principal basis of $se(3)$" as defined in [11], the other two can be considered as parasitic. While further analysis of these parasitic motions can be done within the framework of screw theory, it is beyond the scope of the present paper. As far as the present paper is concerned, the above example serves the purpose of demonstrating the ability of the proposed method to correctly identify the independent or principal motions, even in the presence of parasitic motions that could hamper the proper understanding of the DoF otherwise.

4.2. The Agile Eye

The Agile Eye was introduced by Gosselin and Hamel [8] in 1994. It consists of three legs, each leg containing two links, each having the form of a quarter circle connected to others through revolute joints (see Fig. 3). Due to the symmetry incorporated in the geometry, forward kinematic problem becomes very simple, and is in fact solvable in closed form if the end-effector is represented in terms of the orientation variables $\boldsymbol{\phi} = (\phi, \gamma, \psi)^T$, which are respectively the rotations about the Z, Y and X fixed axes. The coordinates of the end-effector are obtained as shown in [27] :

$$\begin{aligned}
{}^0\boldsymbol{p}_1 &= \boldsymbol{R}_Z(\phi)\,\boldsymbol{R}_Y(\gamma)\,\boldsymbol{R}_X(\psi)\,\boldsymbol{r}_1, \quad \text{where } \boldsymbol{r}_1 = (0, -r, 0)^T,\\
{}^0\boldsymbol{p}_2 &= \boldsymbol{R}_Z(\phi)\,\boldsymbol{R}_Y(\gamma)\,\boldsymbol{R}_X(\psi)\,\boldsymbol{r}_2, \quad \text{where } \boldsymbol{r}_2 = (0, 0, -r)^T,\\
{}^0\boldsymbol{p}_3 &= \boldsymbol{R}_Z(\phi)\,\boldsymbol{R}_Y(\gamma)\,\boldsymbol{R}_X(\psi)\,\boldsymbol{r}_3, \quad \text{where } \boldsymbol{r}_3 = (-r, 0, 0)^T.
\end{aligned}$$

The centroid of the triangle formed by ${}^0\boldsymbol{p}_i$ is taken to be the point of interest:

$${}^0\boldsymbol{p} = \frac{1}{3}\left({}^0\boldsymbol{p}_1 + {}^0\boldsymbol{p}_2 + {}^0\boldsymbol{p}_3\right).$$

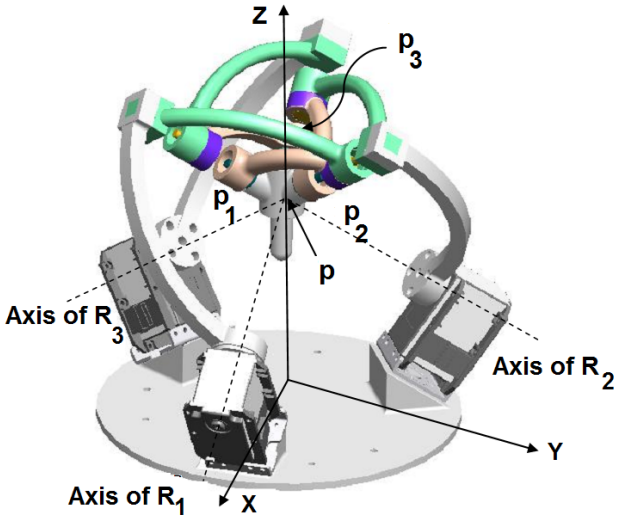

Figure 3: The Agile Eye manipulator

The construction of the Agile Eye is such that the axes of the intermediate joints are orthogonal to the corresponding axes at the end-effector in each leg. These orthogonality conditions lead to the three constraint equations in terms of the unknown variables, $\boldsymbol{\phi}$. The solution to the forward kinematic problem is obtained in closed form and analytical expressions for the unknown variables are obtained. Scaling all the lengths with respect to r, two sample results are presented.

- For active variables $\boldsymbol{\theta} = (\pi/4, -\pi/6, \pi/5)^T$, one set of the unknown variables are given by: $\boldsymbol{\phi}$=$(0.628, 0.088, -2.433)^T$, and the eigenvalues of $\boldsymbol{g}$ are computed as: 0.008, 0.071 and 1.551.
- For $\boldsymbol{\theta} = (\pi/4, \pi/12, \pi/8)^T$ and corresponding $\boldsymbol{\phi}$=$(0.393, -0.083, -2.409)^T$, the eigenvalues of $\boldsymbol{g}$ are 0.066, 0.222 and 0.727.

It can be seen that the end-effector of Agile Eye has three rotational DoF. Therefore as expected, the manipulator belongs to the class $\boldsymbol{\chi}_{30}$ in these configurations.

4.3. The cylindrical manipulator

This parallel manipulator was proposed by Wang and Liu [6]. As shown in Fig. 4, two of the three legs have identical geometry, each consisting of a two-DoF universal joint and two rotary joints. The third leg consists of a planar four-bar parallelogram mechanism and three rotary joints. In this

example, the top moving platform and the fixed base are assumed to be in the form of isosceles triangles. The axes of the revolute joints in legs 1,2,

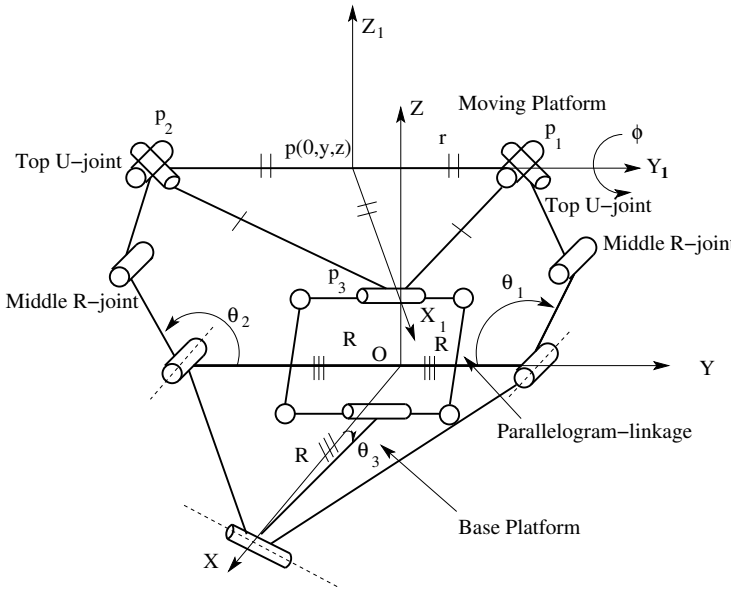

Figure 4: A three-DoF cylindrical manipulator

and the axes of the revolute joints in the four-bar mechanism of the third leg are all parallel to each other, while the axes of the rest of the joints in leg 3 are perpendicular to the aforementioned. The revolute joints attached to the base are actuated and all others are passive. As there are a number of passive joints in this mechanism, an equal number of constraint equations would be required. In order to simplify the task, the end-effector is represented in its task space variables, $\boldsymbol{\phi}=(y, z, \phi)^T$. The coordinates of the end-effector are:

$$
\begin{aligned}
{}^0\boldsymbol{p}_1 &= (0, r+y, z)^T \\
{}^0\boldsymbol{p}_2 &= (0, -r+y, z)^T \\
{}^0\boldsymbol{p}_3 &= (r\cos\phi, y, z+r\sin\phi)^T.
\end{aligned}
$$

The centre of the side ${}^0\boldsymbol{p}_1{}^0\boldsymbol{p}_2$ is taken as the point of interest:

$$
{}^0\boldsymbol{p} = \frac{1}{2}\left({}^0\boldsymbol{p}_1 + {}^0\boldsymbol{p}_2\right).
$$

Using the geometric condition that ${}^0\boldsymbol{p}_1$ and ${}^0\boldsymbol{p}_2$ are confined to move in the YZ plane only and the length of the links adjoining the moving platform remain constant, three constraint equations are framed as shown in [6]. The

expressions for the unknown variables are obtained in the closed form. All the lengths are scaled with respect to R. For $r = 0.6$ and all link lengths equal to 1.2, two sample results are presented:

- For active variables $\boldsymbol{\theta}$=$(-2.171, -1.670, -1.873)^T$ and corresponding unknown variables $\boldsymbol{\phi}$= $(0.37, -2, 0)^T$, the eigenvalues of $\boldsymbol{g}$ are 0, 0 and 5.6372. The matrix

$$\boldsymbol{J_V} = \begin{bmatrix} -1.864 & 2.230 \\ 0 & 0 \\ -1.935 & 1.081 \end{bmatrix}.$$

  The eigenvalues of $\boldsymbol{g_V}$ are 0.408 and 12.954.

- For $\boldsymbol{\theta}$=$(-2.609, -1.813, 0.019)^T$ and $\boldsymbol{\phi}$= $(1/2, -1, 2/5)^T$, the eigenvalues of $\boldsymbol{g}$ are 0, 0 and 15.639. The matrix

$$\boldsymbol{J_V} = \begin{bmatrix} 0.801 & 0.001 \\ 0 & 0 \\ 0.664 & 1.076 \end{bmatrix}.$$

  The eigenvalues of $\boldsymbol{g_V}$ are 0.404 and 1.837.

It can be seen that the moving platform of the cylindrical manipulator has one rotational DoF, and the other two DoF being translational in these configurations. Therefore, the manipulator belongs to the class $\boldsymbol{\chi}_{12}$ in these configurations, which is *complementary* to the class of the 3-R$\underline{\text{P}}$S manipulator.

4.4. MaPaMan-I

The MaPaMan was introduced by Srivatsan and Bandyopadhyay in 2012 [10]. Each of the three legs of MaPaMan consists of a four-bar mechanism at its base, and a strut. The strut is connected to the coupler link by means of a rotary joint, and the top platform by a spherical joint respectively, as shown in Fig. 5. The *crank* of the four-bars are actuated and all other joints are passive. MaPaMan has two different assembly configurations, named MaPaMan-I and MaPaMan-II. In the MaPaMan-I, the strut is in the same plane as the four-bar. The coordinates of the tip of each leg are obtained as:

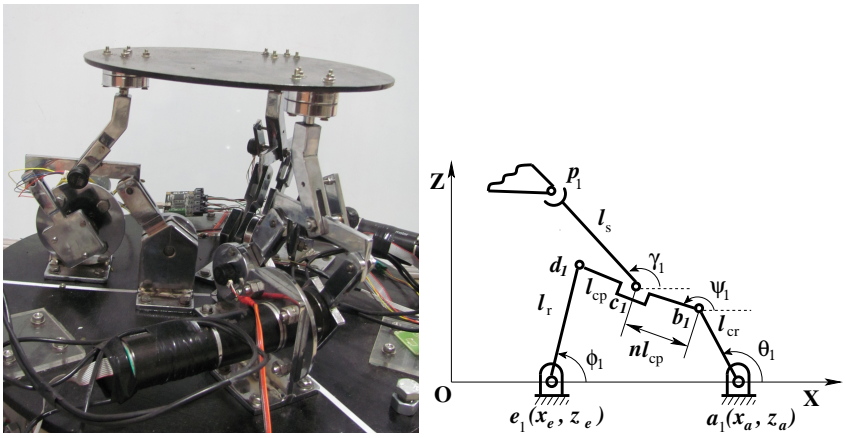

(a) Prototype of MaPaMan-I (b) Schematic of a single leg

Figure 5: Physical prototype and leg architecture of MaPaMan-I

$$
{}^0\boldsymbol{p}_1 = \begin{bmatrix} x_a + l_{cr}\cos\theta_1 + nl_{cp}\cos\psi_1 + l_s\cos\gamma_1 \\ 0 \\ z_a + l_{cr}\sin\theta_1 + nl_{cp}\sin\psi_1 + l_s\sin\gamma_1 \end{bmatrix},
$$

$$
{}^0\boldsymbol{p}_2 = \boldsymbol{R}_Z\,(2\pi/3) \begin{bmatrix} x_a + l_{cr}\cos\theta_2 + nl_{cp}\cos\psi_2 + l_s\cos\gamma_2 \\ 0 \\ z_a + l_{cr}\sin\theta_2 + nl_{cp}\sin\psi_2 + l_s\sin\gamma_2 \end{bmatrix},
$$

$$
{}^0\boldsymbol{p}_3 = \boldsymbol{R}_Z\,(4\pi/3) \begin{bmatrix} x_a + l_{cr}\cos\theta_3 + nl_{cp}\cos\psi_3 + l_s\cos\gamma_3 \\ 0 \\ z_a + l_{cr}\sin\theta_3 + nl_{cp}\sin\psi_3 + l_s\sin\gamma_3 \end{bmatrix}.
$$

The point of interest ${}^0\boldsymbol{p}$ chosen as the centroid of the moving platform is:

$$
{}^0\boldsymbol{p} = \frac{1}{3}\left({}^0\boldsymbol{p}_1 + {}^0\boldsymbol{p}_2 + {}^0\boldsymbol{p}_3\right). \tag{22}
$$

For a given set of inputs $\boldsymbol{\theta}$=$(\theta_1, \theta_2, \theta_3)^T$, the passive variables $\boldsymbol{\psi} = (\psi_1, \psi_2, \psi_3)^T$ are obtained from the forward kinematics of the four-bar. There are three more passive variables to be computed: $\boldsymbol{\phi}$=$(\gamma_1, \gamma_2, \gamma_3)^T$. The three constraint equations $\boldsymbol{\eta} = \boldsymbol{0}$, to solve for the passive variables are given by:

$$
\begin{aligned}
\eta_1 &= ({}^0\boldsymbol{p}_2 - {}^0\boldsymbol{p}_1)\cdot({}^0\boldsymbol{p}_2 - {}^0\boldsymbol{p}_1) - d_t^2, \\
\eta_2 &= ({}^0\boldsymbol{p}_3 - {}^0\boldsymbol{p}_2)\cdot({}^0\boldsymbol{p}_3 - {}^0\boldsymbol{p}_2) - d_t^2, \\
\eta_3 &= ({}^0\boldsymbol{p}_1 - {}^0\boldsymbol{p}_3)\cdot({}^0\boldsymbol{p}_1 - {}^0\boldsymbol{p}_3) - d_t^2,
\end{aligned}
$$

where ${}^0\boldsymbol{p}_i,\ i = 1, 2, 3$, are the position vectors of the three points on the moving platform where the legs are connected, and d_t is the distance between

any two of them. The forward kinematics of this manipulator yields a 16-degree univariate polynomial [10], which is then solved for the given values of actuated variables and the eigenvalues of the matrix $\boldsymbol{g}$ are calculated. All

Table 1: Geometric parameters of the MaPaMan-I and MaPaMan-II

Parameter	Symbol	Value
Crank length	l_{cr}	1/2
Coupler length	l_{cp}	2/3
Rocker length	l_r	1/2
Strut length	l_s	7/10
Strut position	n	1/2
Crank base position	$\boldsymbol{a}$	$(1,0,0)^T$
Rocker base position	$\boldsymbol{e}$	$(1/3,0,0)^T$
End-effector side	d_t	1.155

the lengths are scaled with respect to the distance of the crank base from the origin of the base platform. At two typical non-singular configurations and for the link lengths given in Table 1, the following results are obtained:

- For active variables $\boldsymbol{\theta}$=$(0.8, 1.4, 1.1)^T$ and corresponding $\boldsymbol{\phi}$=$(2.122, 1.705, 1.892)^T$, the eigenvalues of $\boldsymbol{g}$ are: 0, 0.528 and 2.778. The vector $\boldsymbol{J_V} = (0, 0, 0.066)^T$.
- For $\boldsymbol{\theta}$=$(1, 2, 1.5)^T$, $\boldsymbol{\phi}$= $(1.973, 1.266, 1.628)^T$ the eigenvalues of $\boldsymbol{g}$ are: 0,0.079 and 0.269. The vector $\boldsymbol{J_V} = (0, 0, -0.015)^T$.

It is seen that two eigenvalues of $\boldsymbol{g}$ are non-zeros and one eigenvalue is zero. This implies that the moving platform has two rotational DoF and one pure translational DoF. Hence this configuration of the manipulator belongs to the class $\boldsymbol{\chi}_{21}$, the same as the 3-R$\underline{\text{P}}$S. Also, the vector $\boldsymbol{J_V}$ indicates that the pure translation is along the Z-axis, for the same reason as in 3-R$\underline{\text{P}}$S.

4.5. MaPaMan-II

The architecture of the MaPaMan-II is almost the same as that of MaPaMan-I, except that the axis of the revolute joint between the coupler of the four-bar and the strut lies in the plane of the four-bar in the case of the MaPaMan-II (see Fig. 6). The points at the tip of each leg are obtained as:

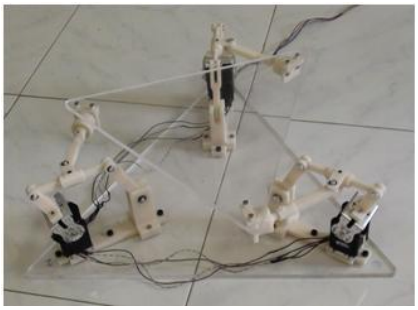

(a) Prototype

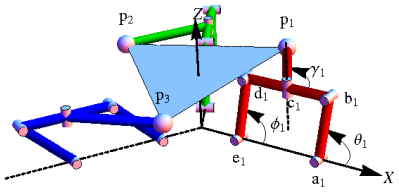

(b) CAD model

Figure 6: CAD model and physical prototype of MaPaMan-II

$$
{}^0\boldsymbol{p}_1 = \begin{bmatrix} x_a + l_{cr}\cos\theta_1 + nl_{cp}\cos\psi_1 + l_s\cos^2\psi_1\cos\gamma_1 + l_s\cos\psi_1\sin\psi_1\sin\gamma_1 \\ l_s\cos\gamma_1\sin\psi_1 - l_s\sin\gamma_1\cos\psi_1 \\ z_a + l_{cr}\sin\theta_1 + nl_{cp}\sin\psi_1 + l_s\cos\psi_1\sin\psi_1\cos\gamma_1 + l_s\sin^2\psi_1\sin\gamma_1 \end{bmatrix},
$$

$$
{}^0\boldsymbol{p}_2 = \boldsymbol{R}_Z\,(2\pi/3) \begin{bmatrix} x_a + l_{cr}\cos\theta_2 + nl_{cp}\cos\psi_2 + l_s\cos^2\psi_2\cos\gamma_2 + l_s\cos\psi_2\sin\psi_2\sin\gamma_2 \\ l_s\cos\gamma_2\sin\psi_2 - l_s\sin\gamma_2\cos\psi_2 \\ z_a + l_{cr}\sin\theta_2 + nl_{cp}\sin\psi_2 + l_s\cos\psi_2\sin\psi_2\cos\gamma_2 + l_s\sin^2\psi_2\sin\gamma_2 \end{bmatrix},
$$

$$
{}^0\boldsymbol{p}_3 = \boldsymbol{R}_Z\,(4\pi/3) \begin{bmatrix} x_a + l_{cr}\cos\theta_3 + nl_{cp}\cos\psi_3 + l_s\cos^2\psi_3\cos\gamma_3 + l_s\cos\psi_3\sin\psi_3\sin\gamma_3 \\ l_s\cos\gamma_3\sin\psi_3 - l_s\sin\gamma_3\cos\psi_3 \\ z_a + l_{cr}\sin\theta_3 + nl_{cp}\sin\psi_3 + l_s\cos\psi_3\sin\psi_3\cos\gamma_3 + l_s\sin^2\psi_3\sin\gamma_3 \end{bmatrix}.
$$

After finding ${}^0\boldsymbol{p}_1$,${}^0\boldsymbol{p}_2$ and${}^0\boldsymbol{p}_3$, the same procedure as that adopted for MaPaMan-I (Section 4.4) is followed and all the passive variables are computed. At two typical non-singular configurations and for the link lengths given in Table 1, the following results are obtained:

- For active variables $\boldsymbol{\theta}$= $(0.8, 1.4, 1.1)^T$ and passive variables $\boldsymbol{\phi}$=$(2.534, 2.238, 2.147)^T$, the eigenvalues of $\boldsymbol{g}$ are: 0.018, 0.075 and 0.151.
- For $\boldsymbol{\theta}$= $(1, 2, 1.5)^T$, $\boldsymbol{\phi}$=$(2.543, 1.966, 1.879)^T$, the eigenvalues of $\boldsymbol{g}$ are: 0.010, 0.029 and 0.155.

As there are no vanishing eigenvalues of $\boldsymbol{g}$, this manipulator has all three rotational DoF and belongs to the class $\boldsymbol{\chi}_{30}$, the same as Agile Eye.

4.6. Summary of observations

In the above analysis, for the configurations studied, the classification of the manipulators emerges as follows: 3-RPS and MaPaMan-I belongs to the

class $\boldsymbol{\chi}_{21}$, Agile Eye and MaPaMan-II belong to $\boldsymbol{\chi}_{30}$, while the cylindrical manipulator alone belongs to the class $\boldsymbol{\chi}_{12}$. However there are quantitative differences within the same class – which, though not the primary focus of this paper – is nevertheless mentioned here in brief for the sake of completeness. In the Agile Eye, the platform is known to have a *spherical motion*, i.e., the platform can only rotate about the stationary point O where the axes of the rotary joints R_1, R_2, R_3 meet (see Fig. 3). However, in MaPaMan-II, the motion is not spherical; in addition to rotating about the three spatial axes, the platform also has some translational motions along these, which are sometimes called the *parasitic motions* in such lower mobility platforms.

5. Gain singularity and the analysis of the gained degree(s)-of-freedom

The results of the study of partitioning of DoF shown in Section 4 are for the manipulators at non-singular configurations. The approach developed in Section 3 is followed in this section to analyse the gained DoF, at the gain-type singularities.

5.1. Gain of single DoF

In the following the gained DoF is characterised when the manipulator gains a single DoF.

5.1.1. The 3-RPS *manipulator*

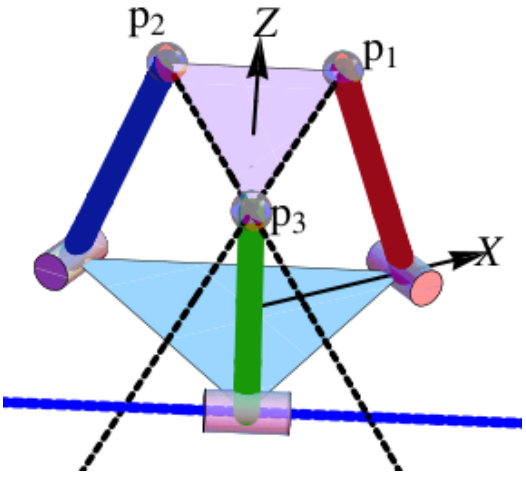

Figure 7: The 3-RPS manipulator in a gain-singular configuration resulting in the gain of a single DoF

The condition for gain-type singularities is adopted from [28], i.e., the manipulator gains one DoF when one of the legs lie in the same plane as the moving platform, as shown in Fig. 7. This configuration is given by: $\boldsymbol{\theta} = (0.770, 1, 1)^T$ and $\boldsymbol{\phi} = (0.606, 1.047, 1.047)^T$. The resulting eigenvalues of $\boldsymbol{J}_{\boldsymbol{\eta\phi}}^T \boldsymbol{J}_{\boldsymbol{\eta\phi}}$ are computed as: 0, 2.595, 5.967; hence nullity($\boldsymbol{J}_{\boldsymbol{\eta\phi}}$)=1. The gained passive velocity is computed as $\dot{\boldsymbol{\phi}}_1^N = (1, 0, 0)^T$. The gained velocities in the task space are:

$$
\begin{aligned}
{}^0\boldsymbol{\omega}_1^N &= (0, -1.026, 0)^T, \quad \text{and} \\
{}^0\boldsymbol{v}_1^N &= (0.1462, 0, 0.211)^T,
\end{aligned}
$$

implying that the gained DoF is *rotational*.

5.1.2. The Agile Eye

The condition for gain-type singularity for this manipulator is given in [27], wherein one of the legs is fully extended or folded. At the configuration given by $\boldsymbol{\theta} = (\pi/2, 0, \pi/6)^T$ and $\boldsymbol{\phi} = (\pi/6, -\pi/2, -2\pi/3)^T$, the eigenvalues of $\boldsymbol{J}_{\boldsymbol{\eta\phi}}^T \boldsymbol{J}_{\boldsymbol{\eta\phi}}$ are -1, -1, 0; i.e., the nullity($\boldsymbol{J}_{\boldsymbol{\eta\phi}}$)=1. The gained passive velocity $\dot{\boldsymbol{\phi}}_1^N = (0, 1, 0)^T$. The gained velocities in the task space are:

$$
\begin{aligned}
{}^0\boldsymbol{\omega}_1^N &= (-1/2, \sqrt{3}/2, 0)^T, \quad \text{and} \\
{}^0\boldsymbol{v}_1^N &= (-0.288, -0.166, 0.455)^T.
\end{aligned}
$$

The results imply that the gained DoF is *rotational*.

5.1.3. The Cylindrical manipulator

The condition for gain type singularity in this case is described in [6]. At the configuration given by $\boldsymbol{\theta} = (0.891, 0.278, 0.585)^T$ and $\boldsymbol{\phi} = (1.263, 1.570, 0)^T$, the eigenvalues of $\boldsymbol{J}_{\boldsymbol{\eta\phi}}^T \boldsymbol{J}_{\boldsymbol{\eta\phi}}$ are: -2.054, 0 and 1.613; i.e., the nullity($\boldsymbol{J}_{\boldsymbol{\eta\phi}}$)=1. The gained passive velocity is $\dot{\boldsymbol{\phi}}_1^N = (0, 0, 1)^T$. The gained velocities in the task space are:

$$
\begin{aligned}
{}^0\boldsymbol{\omega}_1^N &= (1/\sqrt{2}, 1/\sqrt{2}, 0)^T, \quad \text{and} \\
{}^0\boldsymbol{v}_1^N &= (0, -1/5, 0)^T,
\end{aligned}
$$

implying that the gained DoF is *rotational*.

5.1.4. MaPaMan-I

The gain-type singularity condition for MaPaMan-I is adopted from [29]; i.e., the strut lies in the same plane as the moving platform. At the configuration given by (see Fig. 8), $\boldsymbol{\theta} = (1.17466, 1.17466, 0.6266)^T$ and $\boldsymbol{\phi} =$

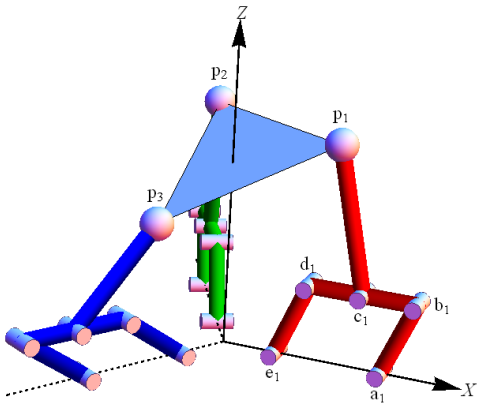

Figure 8: The MaPaMan-I manipulator in a configuration with gain of a single DoF

$(2.175, 2.175, 2.6135)^T$, the eigenvalues of $\boldsymbol{J}_{\boldsymbol{\eta\phi}}^T \boldsymbol{J}_{\boldsymbol{\eta\phi}}$ are: 0, 1.327 and 2.174; i.e., the nullity($\boldsymbol{J}_{\boldsymbol{\eta\phi}}$)=1. The gained passive velocities is computed as $\dot{\boldsymbol{\phi}}_1^N = (0, 0, 1)^T$. The gained velocities in the task-space are:

$$
\begin{aligned}
{}^0\boldsymbol{\omega}_1^N &= (0.606, -0.35, 0)^T, \quad \text{and} \\
{}^0\boldsymbol{v}_1^N &= (0.058, 0.102, -0.201)^T.
\end{aligned}
$$

This implies that the gained DoF is *rotational*.

5.2. Gain of two DoF

In this section, a gain of two-DoF is characterised with the example of the 3-RPS manipulator. The configuration leading to the gain of two DoF requires that $\Delta \boldsymbol{p}_1\boldsymbol{p}_2\boldsymbol{p}_3$ be similar to $\Delta \boldsymbol{g}_1\boldsymbol{p}_2\boldsymbol{g}_3$, and that these triangles lie in the same plane, while the line $\boldsymbol{g}_1\boldsymbol{g}_3$ and point $\boldsymbol{p}_2$ lie on opposite sides of the line $\boldsymbol{p}_1\boldsymbol{p}_3$ (see Fig. 9). This configuration can be obtained in closed form:

$$
\boldsymbol{\theta} = \left(\frac{15 - \sqrt{15}}{2(-1 + \sqrt{15})}, 3, \frac{15 - \sqrt{15}}{2(-1 + \sqrt{15})} \right)^T,
$$

$$
\boldsymbol{\phi} = \left(2\arctan(\sqrt{c/7}), m, 2\arctan(\sqrt{c/7}) \right)^T, \quad \text{where}
$$

$$
m = 2\arctan\left(\frac{2\sqrt{7}c^{3/2} - 14\sqrt{7c} + 2\sqrt{-1106 + 224\sqrt{15} + 343c - 98c^2 + 7c^3}}{-14c} \right), \quad \text{and}
$$

$$
c = 8 - \sqrt{15}.
$$

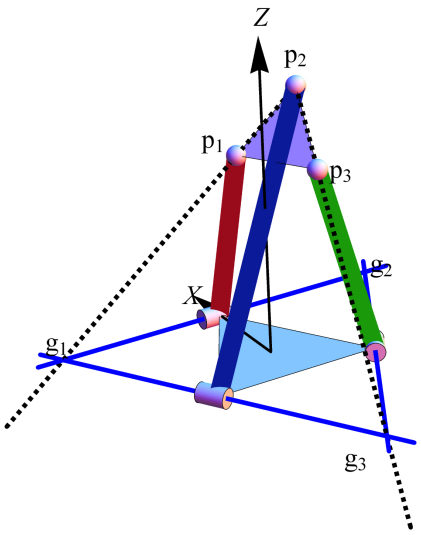

Figure 9: The 3-RPS manipulator in a configuration with gain of two DoF

The resulting eigenvalues of $\boldsymbol{J}_{\boldsymbol{\eta\phi}}^T \boldsymbol{J}_{\boldsymbol{\eta\phi}}$ are: 0, 0, and 15.75; i.e., nullity($\boldsymbol{J}_{\boldsymbol{\eta\phi}}$)=2. The gained passive velocities are:

$$\begin{aligned} \dot{\boldsymbol{\phi}}_1^N &= (-1/\sqrt{2}, 1/\sqrt{2}, 0)^T, \quad \text{and} \\ \dot{\boldsymbol{\phi}}_2^N &= (0, 0, 1)^T. \end{aligned}$$

The gained velocities in the task space are:

$$\begin{aligned} {}^0\boldsymbol{\omega}_1^N &= (0.408248, 1/\sqrt{2}, -1.52797)^T, \\ {}^0\boldsymbol{v}_1^N &= (-0.661438, 0.381881, 0)^T, \\ {}^0\boldsymbol{\omega}_2^N &= (3.4643, -2.00012, 0)^T, \\ {}^0\boldsymbol{v}_2^N &= (-0.41574, -0.720082, 0.555556)^T. \end{aligned}$$

The eigenvalues of $\boldsymbol{g}^N$ are 0.58333 and 1. As $\boldsymbol{g}^N$ has no zero eigenvalues, the manipulator gains two *rotational* DoF in this configuration.

6. Conclusions

This paper presents a formulation to analyse the nature of the DoF in *any* manipulator in general. The same is applied to a class of lower-mobility manipulators, namely, three-DoF spatial parallel manipulators. A general

framework for the formulation of the Jacobian matrices required in the analysis is presented first. Later, it is shown how these matrices can be analysed to determine the partitioning of the DoF in these manipulators. In the same framework, the nature of the DoF gained at a gain-type singularity is analysed. The mathematical formulations are illustrated by applications to several well-known, as well as newly developed parallel manipulators.

References

[1] J. J. Craig, Introduction to Robotics: Mechanics and Control, 2nd Edition, Addison Wesley, California, 1986.

[2] D. Stewart, A platform with six degrees of freedom, in: Proceedings of Instrumentation Mechanical Engineers, 1965-66, pp. 371–386.

[3] H. Makino, N. Furuya, SCARA robot and its family, in: Proceedings of International Conference on Assembly Automation, 1982, pp. 433–444.

[4] R. Clavel, Delta, a fast robot with parallel geometry, in: Proceedings of the 18th International Symposium on Industrial Robots, Springer-Verlag, New York, 2006, pp. 91–100.

[5] K. M. Lee, D. Shah, Kinematic analysis of a three-degrees-of-freedom in-parallel actuated manipulator, IEEE Journal of Robotics and Automation 4 (3) (1988) 354–360.

[6] J. Wang, X.-J. Liu, Analysis of a novel cylindrical 3-DoF parallel robot, Robotics and Autonomous Systems 42 (1) (2003) 31–46.

[7] L.-W. Tsai, Kinematics of a three-dof platform with three extensible limbs, in: Recent Advances in Robot Kinematics, Springer Netherlands, 1996, pp. 401–410.

[8] C. M. Gosselin, J. franois Hamel, The Agile Eye: A High-Performance Three-Degree-of-Freedom Camera-Orienting Device, in: Proceedings of 1994 IEEE International Conference on Robotics and Automation, 1994, pp. 781–787. doi:10.1109/ROBOT.1994.351393.

[9] M. Ceccarelli, A new 3 D.O.F. spatial parallel mechanism, Mechanism and Machine Theory 32 (8) (1997) 895–902.

[10] R. A. Srivatsan, S. Bandyopadhyay, On the position kinematic analysis of MaPaMan: A reconfigurable three-degrees-of-freedom spatial parallel manipulator, Mechanism and Machine Theory 62 (2013) 150–165. doi:10.1016/j.mechmachtheory.2012.11.008.

[11] S. Bandyopadhyay, A. Ghosal, Analytical determination of principal twists in serial, parallel and hybrid manipulators using dual number algebra, Mechanism and Machine Theory 39 (12) (2004) 1289–1305.

[12] G. Gogu, Mobility of mechanisms: a critical review, Mechanism and Machine Theory 40 (9) (2005) 1068–1097. doi:10.1016/j.mechmachtheory.2004.12.014.

[13] K. H. Hunt, Kinematic Geometry of Mechanisms, Clarendon Press, Oxford, 1978.

[14] C. G. Gibson, K. H. Hunt, Geometry of screw systems-1 Screws: genesis and geometry, Mechanism and Machine Theory 25 (1) (1990) 1–10.

[15] Z. Huang, J. Wang, Y. F. Fang, Analysis of instantaneous motions of deficient-rank 3-RPS parallel manipulators, Mechanism and Machine Theory 37 (2) (2002) 229–240.

[16] J. S. Dai, Z. Huang, H. Lipkin, Mobility of overconstrained parallel mechanisms, Journal of Mechanical Design 128 (1) (2006) 220–229. doi:10.1115/1.1901708.

[17] Q. Li, Z. Huang, Mobility analysis of lower-mobility parallel manipulators based on screw theory, in: Proceedings of 2003, IEEE International Conference on Robotics and Automation, Vol. 1, 2003, pp. 1179–1184.

[18] D.-C. Yang, J. Xiong, X.-D. Yang, A simple method to calculate mobility with Jacobian, Mechanism and Machine Theory 43 (9) (2008) 1175–1185. doi:10.1016/j.mechmachtheory.2007.08.001.

[19] S. Bandyopadhyay, Analysis and design of spatial manipulators: an exact algebraic approach using dual numbers and symbolic computation, Ph.D. thesis, Indian Institute of Science, Bangalore, India (2006).

[20] S. Bandyopadhyay, A novel characterisation of spatial manipulators based on their degrees-of-freedom, in: Proceedings of the 2009 IEEE/ASME International Conference on Advanced Intelligent Mechatronics, Singapore, 2009, pp. 618–623. doi:10.1109/AIM.2009.5229944.

[21] C. Gosselin, J. Angeles, Singularity analysis of closed-loop kinematic chains, IEEE Transactions on Robotics and Automation 6 (3) (1990) 281–290. doi:10.1109/70.56660.

[22] S. Bandyopadhyay, A. Ghosal, Analysis of configuration space singularities of closed-loop mechanisms and parallel manipulators, Mechanism and Machine Theory 39 (5) (2004) 519–544.

[23] A. Ghosal, Robotics: Fundamental Concepts and Analysis, 4th Edition, Oxford University Press, New Delhi, 2009.

[24] R. M. Murray, S. S. Sastry, L. Zexiang, A Mathematical Introduction to Robotic Manipulation, 1st Edition, CRC Press, Inc., Boca Raton, FL, USA, 1994.

[25] B. M. St-Onge, C. Gosselin, Singularity analysis and representation of the general Gough-Stewart platform, International Journal of Robotics Research 19 (3) (2000) 271–288.

[26] Z. Huang, Z. Chen, J. Liu, S. Liu, A 3DOF rotational parallel manipulator without intersecting axes, Journal of Mechanisms and Robotics 3 (2) (2011) 8 pages.

[27] I. A. Bonev, D. Chablat, P. Wenger, Working and assembly modes of the Agile Eye, in: Proceedings of the 2006 IEEE International Conference on Robotics and Automation, Orlando, USA, 2006, pp. 2317–2322.

[28] D. Basu, A. Ghosal, Singularity analysis of platform-type multi-loop spatial mechanisms, Mechanism and Machine Theory 32 (3) (1997) 375–389. doi:10.1016/S0094-114X(96)00033-X.

[29] R. A. Srivatsan, Design, analysis and development of MaPaMan, M. Tech. report, Indian Institute of Technology Madras, Chennai, India (May 2012).

A. Degree-of-freedom-based classification of rigid-body motion

The classification of DoF following the concept of partitioning of DoF, as presented in [20], is reproduced below for the sake of easy reference.

Table 2: Classification of spatial motion based on the partition of DoF

Total DoF	Class	Rotational DoF, rank $(\boldsymbol{g})$	Translational DoF, rank $(\boldsymbol{g_V})$
1	$\boldsymbol{\chi}_{10}$	1	0
	$\boldsymbol{\chi}_{01}$	0	1
2	$\boldsymbol{\chi}_{20}$	2	0
	$\boldsymbol{\chi}_{11}$	1	1
	$\boldsymbol{\chi}_{02}$	0	2
3	$\boldsymbol{\chi}_{30}$	3	0
	$\boldsymbol{\chi}_{21}$	2	1
	$\boldsymbol{\chi}_{12}$	1	2
	$\boldsymbol{\chi}_{03}$	0	3
4	$\boldsymbol{\chi}_{31}$	3	1
	$\boldsymbol{\chi}_{22}$	2	2
	$\boldsymbol{\chi}_{13}$	1	3
5	$\boldsymbol{\chi}_{32}$	3	2
	$\boldsymbol{\chi}_{23}$	2	3
6	$\boldsymbol{\chi}_{33}$	3	3
$n,\ n > 6$	$\boldsymbol{\chi}^n_{33}$	3	3